Fabrication and characterization of hydroxyapatite reinforced with 20 vol % Ti particles for use as hard tissue replacement

C. CHU*, P. LIN, Y. DONG
Department of Mechanical Engineering, Southeast University, Nanjing 210018, China
X. XUE
Zhongda Hospital, School of Medicine, Southeast University, Nanjing 210018, China
J. ZHU, Z. YIN
School of Materials Science and Engineering, Harbin Institute of Technology, Box 433, Harbin 150001, China
E-mail: chenglin-chu@263.net

Hydroxyapatite(HA)-based composite reinforced with 20 vol % titanium (Ti) particles was fabricated by hot pressing based on the studies of the structural stability of HA phase in HA–Ti composite by means of FTIR spectrometry and X-ray diffractometry. The mechanical properties and biological behaviors of the composite were investigated by mechanical and *in vivo* studies. The existence of Ti metal phase can promote the dehydration and decomposition of HA ceramic phase into the more stable calcium phosphate phases, such as α–$Ca_3(PO_4)_2$ (α–TCP) and $Ca_4O(PO_4)_2$ at high temperatures. Comparing with pure HA ceramic manufactured under the same conditions, HA–20 vol % Ti composite with higher fracture toughness (0.987 MPa $m^{1/2}$), bending strength (78.59 MPa), work of fracture (12.8 J/m^2), porosity (9.8%) and lower elastic modulus (75.91 GPa) is more suitable for use as hard tissue replacement. Crack deflection is the chief toughening mechanism in the composite. Histological evaluation by light microscope shows HA–20 vol % Ti composite implant could be partially integrated with newborn bone tissues after 3 weeks and fully osteointegrated at 12 weeks *in vivo*. The excellent biological properties of HA–20 vol % Ti composite may be contributed to the coexistence of high porosity and the decomposition products of HA phase in the composite.

1. Introduction

From the point of view of biocompatibility, hydroxyapatite (HA) seems to be the most suitable ceramic for hard tissue replacement. HA (chemical formula $Ca_{10}(PO_4)_6(OH)_2$) is the main mineral constituent of teeth and bones. It does not exhibit any cytoxic effects and shows excellent biocompatibility with hard tissues and also with skin and muscle tissues [1]. Moreover, HA can bond to bone directly [1]. Unfortunately, HA ceramic cannot presently be used for heavy load-bearing applications, like artificial teeth or bones because of its poor mechanical properties and low reliability, especially in wet environments [2]. Some reviews written by Hench [3], Williams [4] and Suchanek and Yoshimura [5] have also discussed these topics. Fabrication of HA ceramic composites can partially solve this problem [5, 6]. A very good example is polyethylene (PE)–HA composite developed by Bonfield [7], which has mechanical properties similar to those of bones.

In recent years, many reinforcements, including particles [8], whiskers [9] and long fibers [10] have been used in HA ceramic to improve its mechanical reliability. Although significant toughening effect has been reported for whisker-reinforced HA-based composites [5], many commercially available whiskers do not pass the so-called Stanton and Pott criterion [11, 12] and are considered as potentially carcinogenic materials. (According to this criterion, the carcinogenic effect of the fibrous materials is restricted to long and thin fibers: diameter $< 1\,\mu m$, length $< 10\,\mu m$). Additionally it is very difficult to be fabricated for long fiber-reinforced HA-based composites [5]. Therefore, particle reinforcement is the relatively preferable choice for HA-based composites. Particle reinforcement materials should have high strength and toughness, good biocompatibility and corrosion resistance. Some bioinert metals, such as silver [13, 14], and ceramics, such as ZrO_2 [15, 16], Al_2O_3 [17, 18] and SiC [19] can meet these requirements.

*Author to whom all correspondence should be addressed.

Among them, metal particle reinforcements present significant toughening effect by energy-absorbing mechanism due to the plastic deformation of ductile metal particles at the tips of cracks [13, 14].

As we know, titanium (Ti) and its alloys are the preferred metal materials for orthopedics and dentistry because of their good biocompatibility [20, 21]. Therefore, the utilization of Ti particles as the reinforcement can improve mechanical properties of HA biomaterials and has little influence on its biological properties. At present, systematic studies on HA-based composites reinforced with Ti particles have not been reported. The purposes of this study were to fabricate HA-based composite reinforced with 20 vol % Ti particles by hot-pressing based on the studies of the structural stability of HA phase in HA–Ti composite by means of FTIR spectrometry and X-ray diffractometry. The mechanical properties and biological behaviors of the composite were investigated by mechanical and *in vivo* studies.

2. Materials and methods

2.1. Raw materials and powder processing

The raw materials used were Ti powders and HA powders. The chemical composition of Ti was (wt %): Ti 99.3, Fe 0.039, O 0.35, N 0.035, C 0.025, CL 0.034, H 0.024 and Si 0.0018. HA powders were prepared by the reaction between $Ca(NO_3)_2$ and $(NH_4)_2HPO_4$. Their Ca/P ratio was $1.67 \pm 2.0\%$. Sizing by means of Laser Particle Sizer (OMEC LS-POP(III)) showed Ti particles had a average size of 45.2 μm (93.64 wt % of Ti particles were in the range 37.0–60.0 μm), whereas the average size of HA particles is 1.75 μm (82.12 wt % of HA particles were found to be between 0.35–3.70 μm). There are significant agglomerations of HA powders shown by scanning electron microscopy (SEM). The mixed powders of HA and Ti with 20 vol % Ti in volume fraction were first blended by ball milling for 12 h and then compacted at 200 MPa. Finally, green compacts were hot-pressed at different temperatures under a pressure of 20 MPa in nitrogen atmosphere for 30 min with a heating rate of 10 °C/min and a cooling rate of 6 °C/min.

2.2. Characterization

The IR spectra of pure HA and HA–Ti composites were recorded using FTIR spectrometry (Nicolet 800). Pelleted samples (1 mg spalling composite mixed with 100 mg KBr) were prepared to determine whether OH^- ions of HA phase were lost during the sintering process. The phase constitution was analyzed by X-ray diffraction (XRD). The density of sintered samples was measured accurately using distilled water by Archimedes method. The relative density was calculated using the measured density divided by the theoretical one. Samples for microstructural observations were cut with a diamond saw, and their surfaces were ground and polished. Vickers' hardness was tested on polished surfaces under a load of 98 N. Three-point bending tests were performed to determine elastic modulus, bending strength and fracture toughness. The fracture surfaces of the samples were covered with a thin film of gold by vacuum-deposition and then examined by SEM.

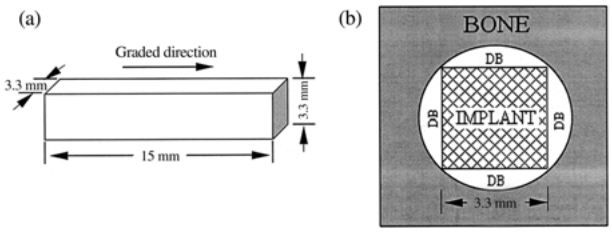

Figure 1 Schematic configuration of the implant model. (a) Rectangular specimen for implantation; (b) Cross-sectional view of the predrilled hole with implant in the skull (DB-defective bone region).

2.3. *In vivo* study

2.3.1. Implant preparation and surgical operation

Pure HA ceramic and HA–Ti composite were cut into rectangular specimens about 3.3 mm × 3.3 mm × 15 mm in dimension using a diamond saw as shown in Fig. 1(a). The rectangular implants were inserted into predrilled holes of 4.76 mm diameter using sterile surgical techniques. The cross-sectional view of the predrilled hole with implant in the skull is illustrated in Fig. 1(b). The defective bone (DB) region was designed for bone healing. Prophylactic antibiotic was given once during operation. Before implantation, all implants were cleaned with distilled water and sterilized by autoclaving at 121 °C for 30 min. A total of 48 implants (24 each of pure HA ceramic and HA–Ti composite) were inserted into the skull of eight New Zealand White rabbits of 2.5 kg weight. With implants randomly distributed, each rabbit contained six implants (three each of pure HA ceramic and HA–Ti composite). After 2, 4, 8 and 12 weeks, two rabbits were sacrificed.

2.3.2. Specimens for histological evaluation

The harvested samples were fixed in 10% buffered formalin. The fixed samples were decalcified in an acid compound (1000 ml solution containing 8.5 g sodium chloride, 100 ml formalin, 70 ml 37% hydrochloric acid, 80 ml formic acid, 40 g aluminum chloride and 25 ml acetic acid glacial). Dehydrated in alcohol and embedded in paraffin, decalcified sections were stained with haematoxylin and eosin (HE) for light microscopic observation. Two samples were used for each histological evaluation at each condition.

3. Results and discussion

3.1. Structural stability of HA phase in HA–20 vol % Ti composite

Manufacture of HA materials by thermal processing involves ionic transport through the apatite structure. The presence of OH^- ions within the structure enables stoichiometric HA to be heated to temperatures as high as 1400 °C [22]. Dehydration due to a lower partial pressure of water at high temperatures can produce oxyhydroxyapatites and also lead to decomposition products of tricalcium phosphate and tetracalcium phosphate

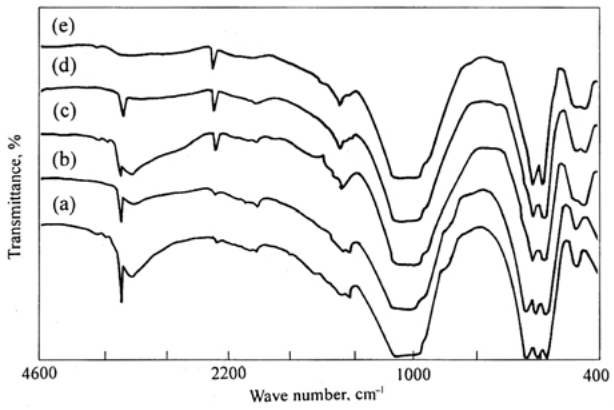

Figure 2 FTIR spectra of pure HA ceramics and HA–20 vol % Ti composites. (a) Raw HA powder; (b) Pure HA bioceramic, 900 °C; (c) Pure HA bioceramic, 1100 °C; (d) HA–20 vol % Ti composites, 900 °C; (e) HA–20 vol % Ti composites, 1000 °C.

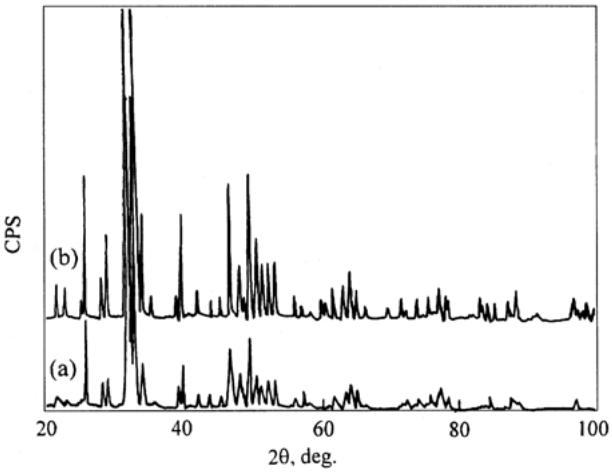

Figure 3 XRD spectra of HA ceramics. (a) Raw HA powders; (b) Pure HA ceramic, treated at 1300 °C for 3 h.

[22, 23]. Moreover, the existence of reinforcements can degrade the structural stability of HA crystal and promote the dehydration and decomposition of HA phase, which can block the densification behaviors of HA composites [8].

Fig. 2 shows FTIR spectra of pure HA and HA–20 vol % Ti composites sintered at different temperatures for 60 min. The infrared spectra of raw HA powders shown in Fig. 2(a) exhibit most bands that have been reported by Baddiel *et al*. [24]. Vibrational frequencies observed of raw HA powders were listed in Table I. For raw HA powders, the vibration peaks of OH^- group are very sharp. Due to hydrogen bonding, the internal antisymmetric stretching vibration of OH^- ions (ν_{OH}) is observed at 3561 cm^{-1}, while the swaying vibration mode of OH^- ions is corresponding to 631 cm^{-1}. A small quantity of CO_3^{2-} groups (corresponding to 1410 cm^{-1} vibration peak) and $(HPO_4)^{2-}$ groups (corresponding to 875 cm^{-1} shoulder shape peak) could be found in raw HA powders. Peak at 1640 cm^{-1} is due to H_2O absorbed by HA. Other vibration peaks are created by PO_4^{3-} groups in HA. Carbonate ions (CO_3^{2-}) substitutes are reported to enhance sinterability of HA ceramic if they replace only phosphate groups in HA lattice [25, 26]. This effect is partially due to coupled substitution with Na and subsequent formation of Na, Ca-phosphates that accelerate the sintering process. On the other hand, CO_3^{2-} for $-OH^-$ substitution has no effect on sintering [26]. CO_3^{2-} do not affect the grain growth of HA during sintering [27]. The presence of various substitutes in HA ceramics significantly affects its performance, not only by influencing the processing conditions, but also by changing chemical properties of the materials, as discussed in detail by LeGeros [28].

Fig. 2(b) shows the IR spectra of pure HA after sintered at 900 °C. It is obvious that the stretching vibration intensity of OH^- ion decreases slightly, while the swaying vibration intensity has no changes. The results show that the HA ceramics begin to lose OH^- ions at 900 °C. Fig. 2(c) indicates that the stretching vibration intensity of OH^- ion in HA ceramics after sintered at 1100 °C decreases markedly, while the swaying vibration cannot already be distinguished. For the latter, only a faint shoulder-shape peak at 630 cm^{-1} appears. It is illuminated that HA ceramics have almost lost all OH^- ions. Fig. 2(d) shows the IR spectra of HA–20 vol % Ti composites sintered at 900 °C. It could be found that although its intensity is very low, the stretching vibration of OH^- ions still exists. A weak shoulder-shape peak corresponding to the swaying vibration presents at 630 cm^{-1}. These indicate that OH^- ions in HA phase have escaped clearly. Fig. 2(e) shows the IR spectra of HA–20 vol % Ti composites sintered at 1000 °C. The stretching vibration of OH^- ions could not already be detected. Only a very faint shoulder-shape peak appears at 630 cm^{-1} due to the swaying vibration, which shows OH^- ions in HA phase have almost escaped entirely. Obviously the existence of Ti metal phase promotes the dehydration reaction of HA phase in HA–20 vol % Ti composites.

Fig. 3 shows XRD spectra of raw HA powders and pure HA ceramic after being sintered at 1300 °C for 3 h in argon atmosphere. Both of them have no impurity phases existing. It is obvious that there are no new phases appearing in pure HA ceramic after sintered at 1300 °C for 3 h. Moreover, each diffraction peak is narrower and sharper and has a higher intensity than that of raw HA powders, which indicated that the crystallinities of treated pure HA ceramic is higher than that of raw HA powders according to Scherrer's theory [29]. Obviously the critical decomposition temperature of raw HA powders used in this paper is above 1300 °C, which is similar to that of HA powders used by Zhou *et al*. [30] and higher than that of HA powders (about 1100–1200 °C) used by Wang and Chaki [31].

Fig. 4 shows XRD spectra of HA–20 vol % Ti composites sintered at different temperatures for

TABLE I Vibrational frequencies observed of raw HA powders (cm^{-1})

Vibrational frequencies	$\nu_1 PO_4$	$\nu_3 F_2 PO_4$	$\nu_4 F_2 PO_4$	ν_{OH}	ν_{OH} stretch	P-OH stretch
HA	959	1120–980	605–550	631	3561	870

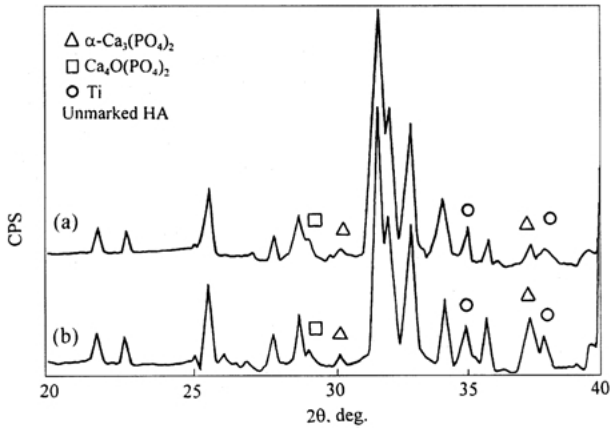

Figure 4 XRD spectra of HA–20 vol % Ti composites sintered at different temperatures for 60 min. (a) 1000 °C; (b) 1100 °C.

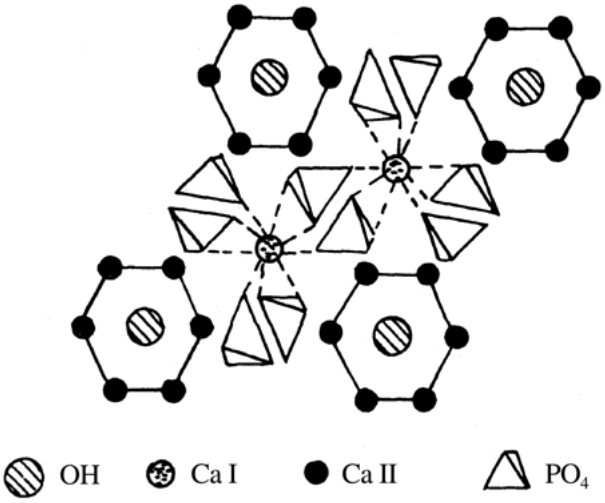

Figure 5 The projection of HA structure on the (0 0 1) plane.

60 min. It is found that a small quantity of decomposition phases, such as $\alpha-Ca_3(PO_4)_2$ (α–TCP) and $Ca_4O(PO_4)_2$ (TCPM) appear in the composite sintered at 1000 °C for 60 min as shown in Fig. 4(a). The intensity of the diffraction peaks due to the decomposition phases in the composite sintered at 1100 °C for 60 min increases, namely, the quantity of decomposition phases increase as shown in Fig. 4(b). At the same time, there were no chemical reactions between HA ceramics and Ti metals, that is to say, no new compounds present. The experimental results are consistent with those reported by the literatures [32, 33]. What kinds of decomposition phases appearing depend on the chemical compositions of HA powders [34, 35]. If Ca/P ratio of HA exceeds 1.67, CaO will emerge during the sintering process. Otherwise, α–β–TCP and $Ca_4O(PO_4)_2$ will appear. The measured value of Ca/P ratio of HA powders used in this paper is 1.66. The decomposition products are consistent with the theoretical results. TCP phase can promote the growth of bone tissue because its degradation rate in the biological environment is faster than that of HA ceramic. Unfortunately, the mechanical instability of the implant increases in this way [3]. In order to improve the bioactivity of the implant materials, a small quantity of TCP phase is allowed to appear in the implant by decomposition reaction of HA phase on the premise of the mechanical guarantee [3, 36].

Among all calcium phosphate ceramics, HA phase is unstable at high temperatures, which is correlative with the features of its crystal structure. Fig. 5 shows the projection of HA structure (S.G. $P6_3/m$) with $a = 0.943$ nm, $c = 0.688$ nm on the (0 0 1) plane, which consists of columns of skewed 3 Ca(II)–O trigonal prisms around the 6_3 axis. It could be found that HA phase has a loosely packed hexagonal structure. A distinct feature of the structure is that the PO_4 tetrahedra do not share the oxygen atoms among them and are held together by the Ca(I) atoms. According to the calculated results of the electrostatic binding energies of different ions present in HA structure by Senger *et al*. [37], the binding energy of OH^- ions in HA structure is the lowest. As a result, OH^- ions can escape from HA lattices first after they acquire enough energies at a high temperature and the dehydration of HA occurs. After the creation of vacancies in the crystal cell, in particular by the departure of two hydroxyl ions, calcium ions become more loosely bound and can then also be displaced, which will lead to the further decomposition of HA phase into the more stable calcium phosphate phase. Obviously both dehydration and decomposition reactions of HA phase are the processes controlled by the kinetics. Their reaction rates are affected by the diffusing rates of the ions in HA lattices. Thus the promoting action of Ti phase on the dehydration and decomposition reactions of HA phase is possibly correlative with the microscopic tensile stress fields in HA matrix induced by Ti particles with a lower sintering shrinkage. Such microscopic tensile stress fields in HA matrix can accelerate the diffusion of the ions in HA lattices and are of benefit for the dehydration and decomposition processes of HA phase controled by the kinetics.

The dehydration and decomposition of HA phase play an important role on the sintering ability of the materials. Oxyhydroxyapatite, the product of dehydration has a better sintering ability than HA phase [31]. So if the decomposition reaction has not happened, the dehydration of HA phase can improve the sintering ability of the materials. On the other hand, the decomposition reaction of HA phase with the generation of new phases can block the sintering densification and deteriorate mechanical properties of the materials [31, 38]. Thus the influence of the Ti metal phase on the dehydration and decomposition of HA phase should be taken into account during the sintering preparation of HA–Ti composites.

3.2. Fabrication and mechanical properties of HA–20 vol % Ti composite

Table II shows the characteristics of HA–20 vol % Ti composite and pure HA ceramic. It could be found that the relative density of pure HA ceramic fabricated by pressureless sintering at 1200 °C reaches 87.6%, while the one of HA–20 vol % Ti composite is only 66.9%. Obviously the sinterability of HA–Ti composite compacts is inferior to that of pure HA powder compacts. This may be due to the promotion of Ti phase on the decomposition of HA ceramics and the difference of sintering shrinkages between HA particles and Ti ones. If the powder compact is isotropic and the relative density of the sample sintered can reach 100%, the linear

TABLE II Characteristics of HA–20 vol %Ti composites and pure HA ceramic

Materials	$\rho_{rel.}$(p-l) (%)	ρ(h-p) (g/cm^3)	$\rho_{rel.}$(h-p) (%)	E (GPa)	σ_{bs} (MPa)	K_{IC} (MPa m$^{1/2}$)	HV (GPa)
Pure HA	0.876	3.161	98.23	110.89	36.86	0.663	4.72
HA–Ti composite	0.669	3.141	90.17	75.91	78.59	0.987	3.13

$\rho_{rel.}$(p-l) – relatively density of materials fabricated by pressureless sintering at 1200 °C.
ρ(h-p) – density of materials sintered by hot-pressing at 1100 °C.
$\rho_{rel.}$(h-p) – relatively density of materials sintered by hot-press at 1100 °C.
E, σ_{bs}, K_{IC} and HV – Young's modulus, bending strength, fracture toughness and Vickers hardness of materials sintered by hot-pressing at 1100 °C.

shrinkage of the compact $(L\%)$ could be acquired by the following expression [39],

$$L\% = 1 - \sqrt[3]{\rho\%} \quad (1)$$

where ρ% is the relative density of the powder compact under a certain pressure. Under a pressure of 200 MPa, the relative densities of pure HA powders and pure Ti powders are 54.6% and 65.3% respectively. Thus the average linear shrinkages of HA and Ti powders in HA–Ti composite compacts are 18.3% and 13.2% respectively. The former is 38.6% larger than the latter. Therefore, to achieve a high sintering density and avoid or reduce the decomposition reaction of HA as much as possible, the sintering temperature of HA–Ti composite should be chosen near the beginning temperature of the decomposition of HA phase. At the same time, hot pressing technique (HP) could be used for this purpose. Based on above studies on the structural stability of HA phase in HA–Ti composite, combining the sintering characteristics of HA matrix and Ti particle reinforcement, the sintering technics for HA–Ti composite was optimized, namely hot pressing at 1100 °C under a pressure of 20 MPa for 30 min [40].

As shown in Table II, the tested density of hot-pressed pure HA ceramic at 1100 °C is close to the theoretical one of HA ceramic. The relative density of this pure HA ceramic reaches 98.13%. The actual density of hot pressed HA–20 vol % Ti composite is 90% of its theoretical density. Fig. 6 shows the microstructure of HA–20 vol % Ti composite, in which the white phase is Ti and the dark one is HA. Obviously Ti metal particles distribute homogeneously in HA ceramic matrix. HA and Ti phases mainly exist in their simple substance in sintered HA–20 vol % Ti composite as shown in Fig. 7, and no reactions between HA and Ti are detected. However, a small quantity of decomposed phases of HA, such as α–$Ca_3(PO_4)_2$ and $Ca_4O(PO_4)_2$ can be found.

Vicker's hardness of this HA–20 vol % Ti composite is 3.13 GPa, which is lower than that of pure HA ceramic due to the lower relative density of HA–20 vol % Ti composite and the lower hardness of Ti phase comparing with pure HA. Elastic modulus of HA–20 vol % Ti composite is 75.91 GPa, which is lower than that of pure HA (110.89 GPa) and far lower than that of ZrO_2 (210 GPa) and Al_2O_3 (380 GPa). From the point of view of the requirements towards the materials for hard tissue replacement implant, a biomaterial with low elastic modulus is anticipated [3]. Because the modulus of natural bones is low (7–25 GPa), an implant with high modulus can cause severe stress concentration, namely load shielding from a natural bone, which may weaken the bone and deteriorate the implant/bone interface.

Bending strength of pure HA is only 36.86 MPa. Strengthened by Ti particle reinforcements, bending strength of HA–20 vol % Ti composite reaches 78.59 MPa, which is twice that of pure HA. Fracture toughness of pure HA is only 0.663 MPa m$^{1/2}$, while the one of HA–20 vol % Ti composite is 0.987 MPa m$^{1/2}$. Work of fracture of the materials (G_{IC}) could be gained by the following expression from fracture toughness (K_{IC}) and elastic modulus (E),

$$G_{IC} = K_{IC}^2/E \quad (2)$$

Work of fracture of pure HA with relatively low fracture toughness and high elastic modulus is only 4.0 J/m^2, which is far lower than that of Al_2O_3 ceramic (38 J/m^2) with $E = 380$ GPa and $K_{IC} = 3.8$ MPa m$^{1/2}$. By contrast,

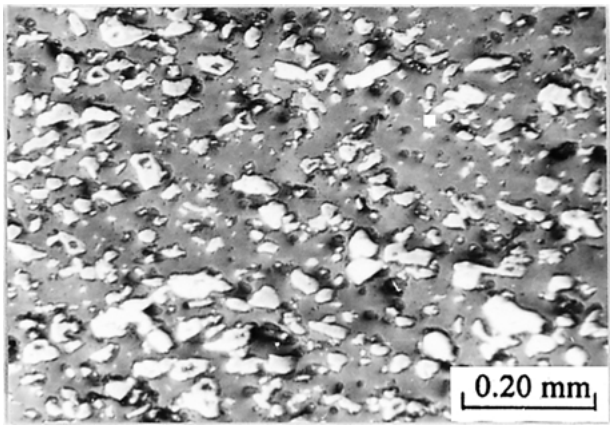

Figure 6 Microstructure of HA–20 vol % Ti composite.

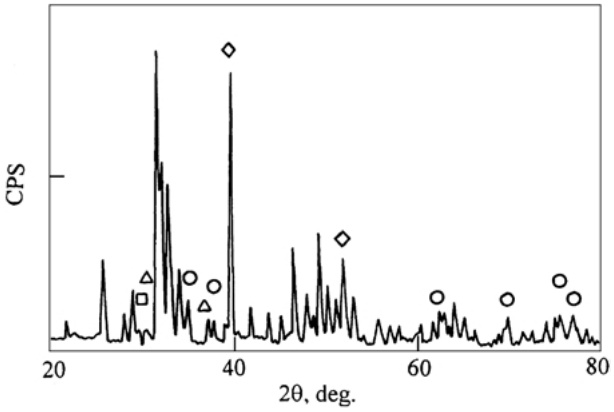

Figure 7 XRD pattern of HA–20 vol % Ti composite. (△) α − $Ca_3(PO_4)_2$, (□) $Ca_4O(PO_4)_2$, (○) Ti, (◇) Ti and HA, (unmarked) HA.

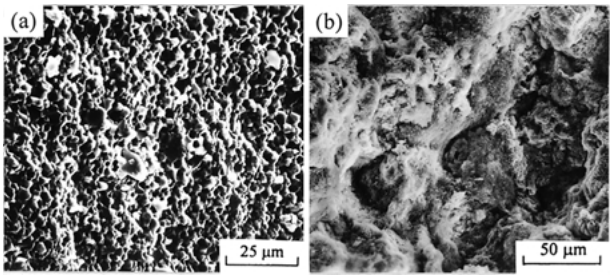

Figure 8 SEM fractographs show fracture surface characteristics of (a) Pure HA ceramic and (b) HA–20 vol % Ti composite.

work of fracture of HA–20 vol % Ti composite with relatively high fracture toughness and low elastic modulus reaches 12.8 J/m^2.

Fracture surface characteristics of pure HA and HA–20 vol % Ti composite were observed by SEM as shown in Figs 8 and 9. It could be found that pure HA presents typical intergranular fracture without macroscopic plastic deformation as shown in Figs 8(a) and 9(a). Cracks propagate on the chief fracture surface and no secondary cracks appear, which indicated that pure HA is very brittle. In HA–20 vol % Ti composite, HA matrix also presents intergranular fracture. Most Ti particles protruding from the fracture surfaces are intact (Fig. 8(b)). Detailed examination (Fig. 9(b)) shows there are many cracks in the HA matrix and large pores left behind due to the pull-out of Ti particles. First, the presence of many cracks in the HA matrix indicates that the HA matrix is very weak. As a consequence, a crack may easily be deflected into the matrix when encountering Ti particles. Second, the pull-out of Ti particles is the result of the crack propagation along the interface, which indicates the interface bonding appears to be weak. If the interface bonding can be improved, the plastic deformation of Ti particles may act more effectively as an energy-absorbing mechanism and toughen the material further. It is obvious that crack deflection is the chief toughening mechanism. The contribution of crack deflection to the toughness can be predicted according to a model [41], to be only about 22–35% of the matrix toughness, while the experimental results show that the toughness of HA–20 vol % Ti composite is 1.56 times that of pure HA, which suggests some other toughening mechanisms, such as the energy-absorbing mechanism of defects which may also arise in HA–20 vol % Ti composite.

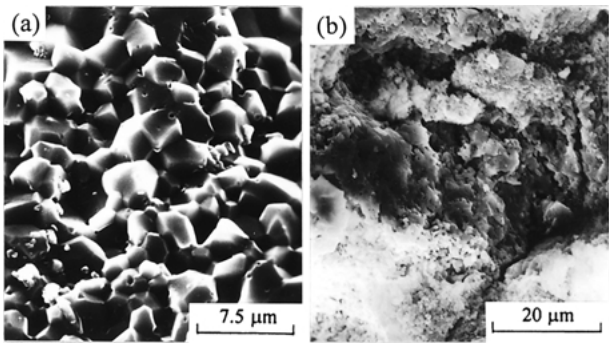

Figure 9 SEM fractographs with high magnification show fracture surface characteristics of (a) pure HA ceramic and (b) HA–20 vol % Ti composite.

Additionally it should be pointed out that mechanical properties of this biological composite can be improved further by composite fabricating techniques, such as hot-pressing combined with liquid phase sintering by the addition of sintering aids [5]. These are our future studying work.

3.3. Biological properties of HA–20 vol % Ti composite

Histological observations after three weeks of the implantation indicate the DB regions between both kinds of implants and host bone were filled with newborn osteoid as shown in Fig. 10(a) and (b), which suggests the biocompatibility and osteoconductivity of HA–20 vol % Ti composite may be very good like those of pure HA bioceramic. On the other hand, it could be found that pure HA implant was fully osteointegrated with newborn bone tissues (Fig. 10(a)). Although the majority of the composite implant could contact with newborn bone directly, the composite implant was only partially integrated with newborn bone because of some fibrous tissues existing at the partial interface between the implant and newborn bone (Fig. 10(b)). This may be due to the decrease of osteointegration ability of the composite implant induced by the existence of bioinert Ti metal phase in the composite during the beginning period of the implantation. As shown in Fig. 11(b), the

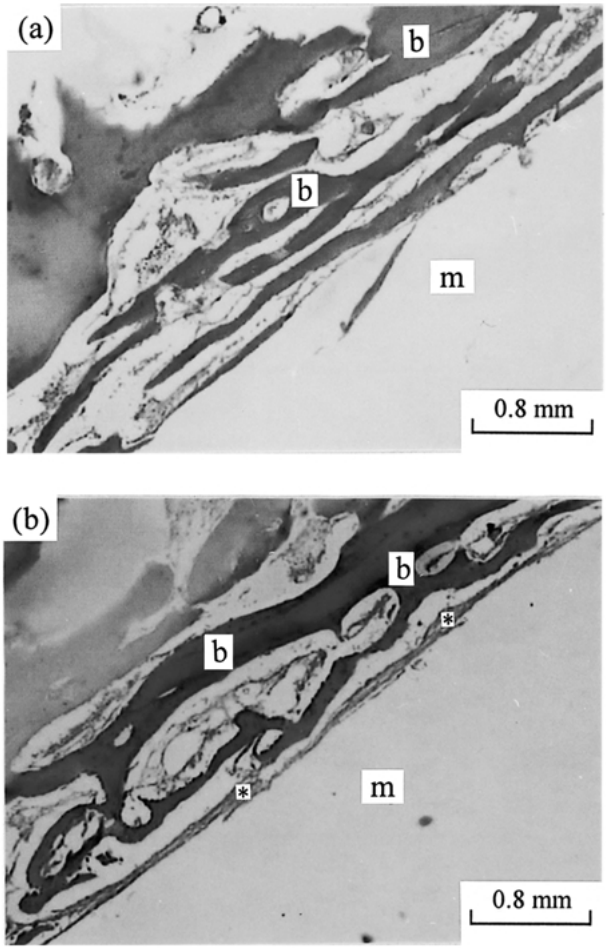

Figure 10 Optical micrograph of bone–implants interface after 3 weeks *in vivo*. (a) Pure HA; (b) HA–20 vol % Ti composite. m, implant; b, newborn bone; *, fibrous tissue.

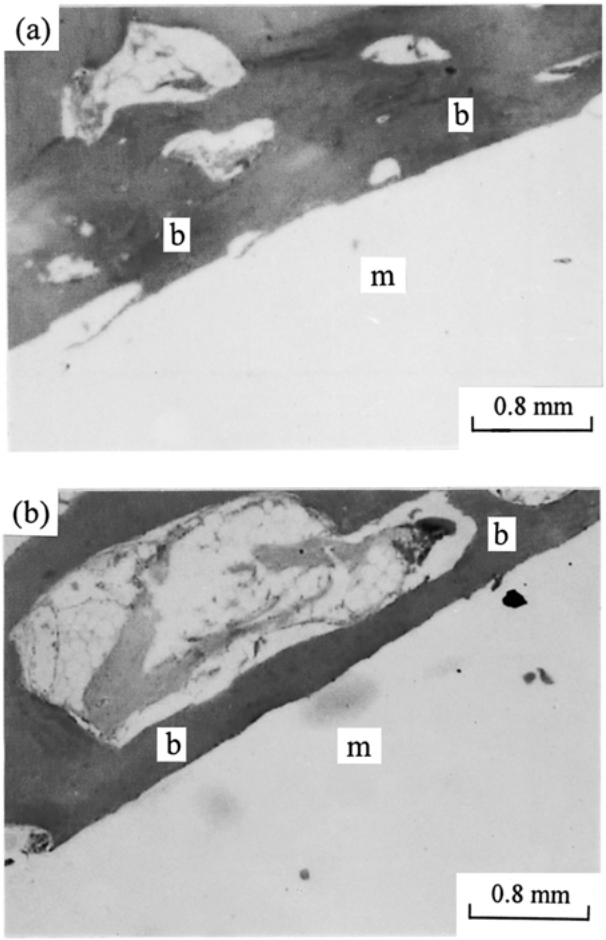

Figure 11 Optical micrograph of bone–implants interface after 12 weeks *in vivo*. (a) Pure HA; (b) HA–20 vol % Ti composite. m, implant; b, newborn bone.

full osteointegration with newborn bone tissues for the composite implant could be attained like pure HA one (Fig. 11(a)) at 12 weeks *in vivo*.

From the point of view of osteointegration ability of the implants with newborn bone tissues after long time *in vivo*, HA–20 vol % Ti composite has almost the same excellent biological properties as pure HA bioceramic. This may be contributed to the coexistence of high porosity and the decomposition products of HA phase in the composite. The porosity of the composite reaches 9.8%, which can improve the bioactivity of the biomaterials effectively [42, 43]. At the same time, the degradation rate of the decomposition products of HA phase, such as α–TCP in the biological environment is faster than that of HA ceramic [3]. The mild dissolution of the decomposition products of HA phase in HA–20 vol % Ti composite can provide a Ca/P environment needed for bone formation [36].

4. Conclusions

The studies on the structural stability of HA phase in HA–Ti composite by means of FTIR spectrometry and X-ray diffractometry shows the existence of Ti metal phase can promote the dehydration and decomposition of HA ceramic phase into the more stable calcium phosphate phases, such as α–$Ca_3(PO_4)_2$ (α–TCP) and $Ca_4O(PO_4)_2$ at high temperatures. The decomposition reaction of HA phase with the generation of new phases and the difference of sintering shrinkages between HA particles and Ti ones can block the sintering densification and deteriorate mechanical properties of the materials.

The HA-based composite reinforced with 20 vol % Ti particles was fabricated by hot-pressing. The applied stress allows us to decrease the temperature and duration required to densify the composite, which can avoid or reduce the decomposition reaction of HA in the composite as much as possible during the sintering process. Comparing with pure HA ceramic manufactured under the same conditions, HA–20 vol % Ti composite with higher fracture toughness (0.987 MPa $m^{1/2}$), bending strength (78.59 MPa), work of fracture (12.8 J/m^2), porosity (9.8%) and lower elastic modulus (75.91 GPa) is more suitable for use as hard tissue replacement. Crack deflection is the chief toughening mechanism in the composite. On the contrary, the strength and toughness of HA–20 vol % Ti composite remain lower than the values of human bone [3, 5]. Therefore, composite technology to strengthen and toughen the materials appears necessary.

Histological evaluation by light microscope shows HA–20 vol % Ti composite implant could be partially integrated with newborn bone tissues after 3 weeks and fully osteointegrated at 12 weeks *in vivo*. The excellent biological properties of HA–20 vol % Ti composite may be contributed to the coexistence of high porosity and the decomposition products of HA phase in the composite.

Acknowledgments

The authors are grateful to Prof. S. Z. Xing, Department of Oral and Maxillofacial Surgery, Stomatological Hospital, Nanjing Medical University, for his kind help in part of the experimental work.

References

1. H. AOKI, *Science and Medical Applications of Hydroxyapatite*, JAAS, Tokyo, 1991.
2. G. DE WITH, H. J. A. VAN DIJK, N. HATTU and K. PRIJS, *J. Mater. Sci.* **16** (1981) 1592.
3. L. L. HENCH, *J. Am. Ceram. Soc.* **74** (1991) 1487.
4. D. F. WILLIAMS, *Mater. Sci. Technol.* **3** (1987) 797.
5. W. SUCHANEK and M. YOSHIMURA, *J. Mater. Res.* **13** (1998) 94.
6. J. M. WU and T. S. YEH, *J. Mater. Sci.* **23** (1988) 3771.
7. W. BONFIELD, in ''Bioceramics: Materials Characteristics vs *In Vivo* Behavior'', Vol. 523, edited by P. Ducheyne and J. E. Lemons (Annals of New York Academy of Science, New York, 1988) p. 173.
8. A. J. RUYS, A. BRANDWOOD, B. K. MILTHORPE, M. R. DICKSON, K. A. ZEIGLER and C. C. SORRELL, *J. Mater. Sci.: Mater. Med.* **6** (1995) 297.
9. W. SUCHANCK, M. YASHIMA, M. KAKIHANA and M. YOSHIMURA, *J. Am. Ceram. Soc.* **80** (1997) 2805.
10. G. DE WITH and A. J. CORBIJN, *J. Mater. Sci.* **24** (1989) 3411.
11. B. T. MOSSMAN, J. BIGNON, M. CORN, A. SEATON and J. B. L. GEE, *Science* **247** (1990) 294.
12. J. D. BIRCHALL, D. R. STANLEY, M. J. MOCKFORD, G. H. PIGOTT and P. J. PINTO, *J. Mater. Sci. Lett.* **7** (1988) 350.
13. X. ZHANG, G. H. M. GUBBELS, R. A. TERPSTRA and R. METSELAAR, *J. Mater. Sci.* **32** (1997) 235.
14. T. K. CHAKI and P. E. WANG, *J. Mater. Sci.: Mater. Med.* **5** (1994) 533.

15. M. TAKAGI, M. MOCHIDA, N. UCHIDA, K. SAITO and K. UEMATSU, *ibid.* **3** (1992) 199.
16. Y. FANG, D. M. ROY, J. CHENG, R. ROY and D. K. AGRAWAL, *Ceram. Trans.* **36** (1993) 397.
17. J. LI, B. FARTASH and L. HERMANSSON, *Interceram.* **39** (1990) 20.
18. H. Y. JUANG and M. H. HON, *Mater. Sci. Eng.* **C2** (1994) 77.
19. T. NOMA, N. SHOJI, S. WADA and T. SUZUKI, *J. Ceram. Soc. Jpn.* **100** (1992) 1175.
20. R. VAN NOORT, *J. Mater. Sci.* **22** (1987) 3801.
21. K. WANG, *Mater. Sci. Eng.* **A213** (1996) 134.
22. K. A. GROSS, C. C. BERNDT, P. STEPHENS and R. DINNEBIER, *J. Mater. Sci.* **33** (1998) 3985.
23. H. J. KLEEBE, E. F. BRES, D. B. ASSOLANT and G. ZIEGLER, *J. Am. Ceram. Soc.* **80** (1997) 37.
24. S. N. VAIDYA and V. SUGANDHI, *J. Mater. Sci.* **34** (1999) 3769.
25. L. G. ELLIES, D. G. A. NELSON and J. D. B. FEATHERSTONE, *J. Biomed. Mater. Res.* **22** (1988) 541.
26. Y. DOI, T. KODA, M. ADACHI, N. WAKAMATSU, T. GOTO, H. KAMEMIZU, Y. MORIWAKI and Y. SUWA, *ibid.* **29** (1985) 1451.
27. A. KRAJEWSKI, A. RAVAGLIOLI, N. ROVERI, A. BIGI and E. FORESTI, *J. Mater. Sci.* **25** (1990) 3203.
28. R. Z. LEGEROS, ''Calcium Phosphates in Oral Biology and Medicine'', (Karger AG, 1991).
29. H. P. KLUG, ''X-ray Diffraction Procedures for Polycrystalline and Amorphous Material'', 2nd edn (New York, 1971) p. 52.
30. J. M. ZHOU, X. D. ZHANG, J. Y. CHEN, S. X. ZENG and K. DE GROOT, *J. Mater. Sci.: Mater. Med.* **4** (1993) 83.
31. P. E. WANG and T. K. CHAKI, *ibid.* **4** (1993) 150.
32. P. VAN LANDUYT, F. LI, J. P. KEUSTERMANS, J. M. STEYDIO, F. DELANNAY and E. MUNTING, *ibid.* **6** (1995) 8.
33. J. WENG, X. G. LIU, X. D. ZHANG and X. Y. JI, *J. Mater. Sci. Lett.* **13** (1994) 159.
34. A. SLOSARCZYK, E. STOBIERSKA, Z. PASZKIEWICZ and M. GAWLICKI, *J. Am. Ceram. Soc.* **79** (1996) 2539.
35. A. ROYER, J. C. VIGUIE, M. HEUGHEBAERT and J. C. HEUGHEBAERT, *J. Mater. Sci.: Mater. Med.* **4** (1993) 76.
36. H. P. YUAN, Z. J. YANG, Y. B. LI, X. D. ZHANG, J. D. DE BRUIJN and K. DE GROOT, *ibid.* **9** (1998) 723.
37. B. SENGER, E. F. BRES, J. L. HUTCHISON, J. C. VOEGEL and R. M. FRANK, *Philosophical Magazine* **A65** (1992) 665.
38. C. L. CHU, J. C. ZHU, Z. D. YIN and S. D. WANG, *Functional Materials* **30** (1999) 606.
39. H. X. JI and P. M. MARQUIS, *J. Mater. Sci.* **28** (1993) 1941.
40. C. L. CHU, ''Fabrication and Microstructure-Properties of Hydroxyapatite/Ti Functionally Graded Biomaterial'', PhD Dissertation, (Harbin Institute of Technology, P. R. China, 2000).
41. K. T. FABER and A. G. EVANS, *Acta. Metall.* **31** (1983) 565.
42. D. M. LIU, *J. Mater. Sci.: Mater. Med.* **8** (1997) 227.
43. I. H. ARITA, V. M. CASTANO and D. S. WILKINSON, *ibid.* **6** (1995) 19.

Received 18 October 2000
and accepted 18 September 2001